Four-component Scattering Power Decomposition with Rotation of Coherency Matrix

Yoshio Yamaguchi, *Fellow, IEEE,* Akinobu Sato, Wolfgang Martin Boerner, *Life Fellow, IEEE,* Ryoichi Sato, *Member, IEEE,* and Hiroyoshi Yamada, *Member, IEEE*

***Abstract*—This paper presents an improvement to a decomposition scheme for accurate classification of polarimetric SAR images. Using a rotation of the coherency matrix to minimize the cross-polarized component, the four-component scattering power decomposition is applied to fully polarimetric SAR images. It is known that oriented urban area and vegetation signatures are decomposed into the same volume scattering mechanism in the previous decompositions and that it is difficult to distinguish vegetation from oblique urban areas with respect to radar direction of illumination within the volume scattering mechanism. It is desirable to distinguish these two scattering mechanisms for accurate classification although they exhibit similar polarimetric responses. The new decomposition scheme by implementing a rotation of coherency matrix first and subsequently the four-component decomposition yields considerably improved accurate results that oriented urban areas are recognized as double bounce objects from volume scattering.**

***Index Terms*—Scattering power decomposition, radar polarimetry, coherency matrix rotation, deorientation, POLSAR, Quad-pol SAR**

I. Introduction

SINCE the launch of ALOS-PALSAR in 2006, a large number of fully polarimetric (Quad-pol) data sets have been acquired from space [1]-[2]. Although the fully polarimetric mode is hitherto an experimental one, it has provided us with precious data sets of various places spread over the planet earth. The total number of scenes exceeds more than 200,000 as of June 2010.

There are various image analysis methods for fully polarimetric data sets [3]-[8]. The representative and fundamental methods are based on incoherent analysis dealing with ensemble averaging of several pixels retaining the second order statistics of polarimetric information. The most frequently used method is the H-Alpha-Anisotropy developed by Cloude and Pottier [3]-[5] based on the eigenvalues of coherency matrix. The second one is the scattering power decomposition method [6]-[8] based on physical scattering models, which was first developed by A. Freeman and S. Durden [6]. The current paper extends the earlier work of the four-component decomposition [8] and employs a rotation of the coherency matrix for more accurate polarimetric synthetic aperture radar (POLSAR) image decomposition and scatterer classification.

The three-component or four-component decomposition scheme divides polarimetric data of the imaging pixel area into surface scattering, double bounce scattering, volume scattering, and helix scattering components. These scattering powers are calculated very easily, and are used to compose full color images with RGB color-coding; Red for the double bounce power, Green for the volume scattering power, and Blue for the surface scattering power, for which each color brightness is corresponding to the magnitude. They have been successfully applied to POLSAR image analysis since color-coded images are easier to understand, and since each color represents a specific scattering mechanism.

However, there exists the following problem in urban area or for man-made structures. Man-made structures such as buildings orthogonal to radar illumination are decomposed into double bounce objects exhibiting "red" in the decomposed image as shown in the Patch A of Fig. 1 (a). The double bounce scattering for this orthogonal illumination is caused by right angle structures consisting of building block walls and road surfaces. The cross-polarized component is small in this orthogonal illumination. The problem appears for oblique urban blocks or man-made structures whose main scattering center is at an oblique direction with respect to radar illumination. If urban blocks are aligned at an oblique angle as shown in the Patch B of Fig. 1 (a), the decomposed image exhibit some mixture of RGB colors in which "green" shows volume scattering. Since the cross-polarized component is created by multiple scattering in these man-made structures for this oblique angle incidence as well as surface scattering from oblique building walls, the ratio of the cross-polarized (HV) component increases in polarimetric radar observations. That is, the magnitude ratio of the HV component becomes large compared to those of the co-polarized HH and VV components for the oblique incidence. Since the HV component mainly contributes to the volume scattering power, these obliquely oriented urban structures are decomposed into volume scattering objects such as trees or vegetation. Since "green" color is allotted for volume scattering in the RGB color-coded image presentation, one may confuse the urban

Manuscript received Nov. 30, 2009; revised April 27, 2010; July 2, 2010, and Nov. 13, 2010; accepted Dec. 5, 2010.

area as vegetation caused by volume scattering. Although these urban structures have strong backscattering power compared to those of vegetation, they are classified as "green" in case the RGB color-coding presentation is used. It is desirable to classify obliquely oriented urban blocks/buildings as man-made structures (red) from the classification point of view as we will see in Fig. 1 (b).

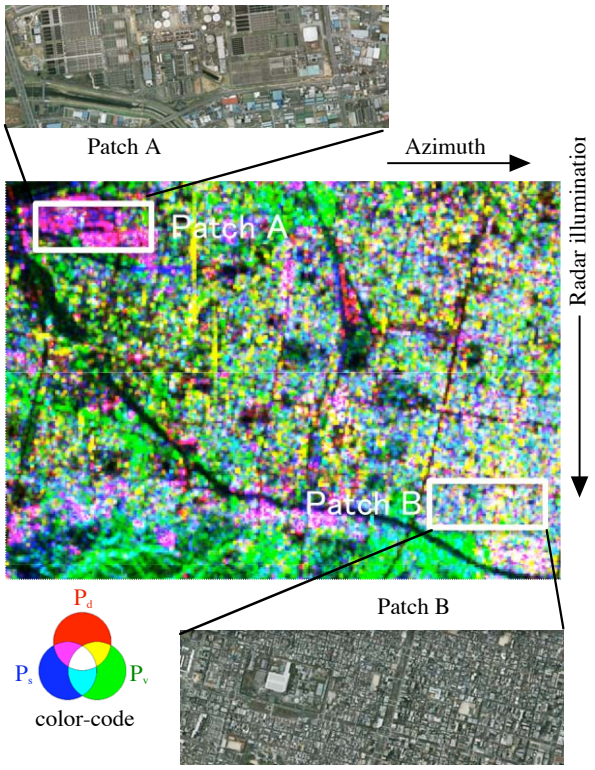

(a) Original color-coded decomposition image with Google Earth optical image (Patch A and B) of unspecified date. Patch A: almost orthogonal to radar illumination, Patch B: oblique to radar illumination.

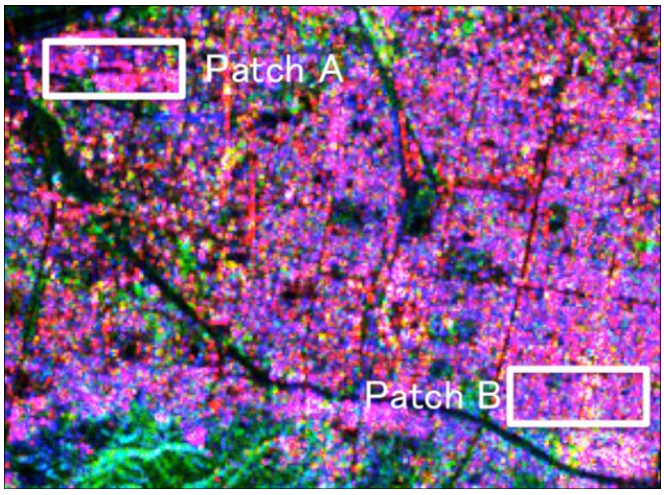

(b) New decomposition image

Fig. 1 Color-coded decomposition image of urban area of Kyoto, Japan, using ALOS PALSAR Quad-pol data

In order to resolve this oblique urban problem, we present in this paper an improvement to a decomposition scheme using an idea of desying first conceived by Huynen [9]. The idea shows that the "Desying operation (elimination of the tilt angle) is one of the major processes that full polarimetric SAR image processing allows one to do" in [3]. The idea is further developed in [10] where the terminology "deorientation" is used. We adopt this concept and apply it to the four-component scattering power decomposition [8].

In the following, the rotation of the coherency matrix, rotation angle, and decomposition scheme using the rotated coherency matrix are described. Some examples are provided to show the effectiveness of the new decomposition scheme.

II. Four-Component Scattering Power Decomposition Based on Measured Coherency Matrix

If scattering matrix data set of the imaging pixel area is acquired, the corresponding coherency matrix can be created, which retains the second order statistics of polarimetric information. The ensemble average of the coherency matrix is given as

$$\langle [T] \rangle = \langle \boldsymbol{k}_P \boldsymbol{k}_P^{\dagger} \rangle, \tag{1}$$

where $\dagger$ denotes complex conjugation and transposition, $< >$ denotes ensemble average, and the Pauli vector is defined as

$$\boldsymbol{k}_P = \frac{1}{\sqrt{2}} \begin{bmatrix} S_{HH} + S_{VV} \\ S_{HH} - S_{VV} \\ 2S_{HV} \end{bmatrix}. \tag{2}$$

Then the measured coherency matrix can be expanded into four sub-matrices which correspond to surface scattering, double bounce scattering, volume scattering, and helix scattering mechanisms

$$\langle [T] \rangle = f_s \langle [T] \rangle_{surface} + f_d \langle [T] \rangle_{double} + f_v \langle [T] \rangle_{vol} + f_c \langle [T] \rangle_{helix} \tag{3}$$

where f_s , f_d , f_v *and* f_c are the expansion coefficients to be determined. These four terms have been derived based on the physical scattering models as shown in Fig. 2 (please see [7] and [8] for more details).

The expansion matrix for the surface scattering is

$$\langle [T] \rangle_{surface} = \begin{bmatrix} 1 & \beta^* & 0 \\ \beta & |\beta|^2 & 0 \\ 0 & 0 & 0 \end{bmatrix}, \quad |\beta| < 1 \tag{4}$$

For the double bounce scattering, the expansion matrix is given by

$$\langle [T] \rangle_{bouble} = \begin{bmatrix} |\alpha|^2 & \alpha & 0 \\ \alpha^* & 1 & 0 \\ 0 & 0 & 0 \end{bmatrix}, \quad |\alpha| < 1 \tag{5}$$

where α *and* β are unknowns to be determined.

For the volume scattering, we employ one of the following matrices according to the magnitude balance of $\langle |S_{HH}|^2 \rangle$ and $\langle |S_{VV}|^2 \rangle$.

$$\langle [T] \rangle_{vol} = \frac{1}{30} \begin{bmatrix} 15 & 5 & 0 \\ 5 & 7 & 0 \\ 0 & 0 & 8 \end{bmatrix}, \quad \text{for } 10 \log \left(\langle |S_{VV}|^2 \rangle / \langle |S_{HH}|^2 \rangle \right) < -2\ dB \tag{6}$$

$$\langle [T] \rangle_{vol} = \frac{1}{4} \begin{bmatrix} 2 & 0 & 0 \\ 0 & 1 & 0 \\ 0 & 0 & 1 \end{bmatrix}, \quad \text{for } \left| 10 \log \left(\langle |S_{VV}|^2 \rangle / \langle |S_{HH}|^2 \rangle \right) \right| < 2\ dB \tag{7}$$

$$\langle [T] \rangle_{vol} = \frac{1}{30} \begin{bmatrix} 15 & -5 & 0 \\ -5 & 7 & 0 \\ 0 & 0 & 8 \end{bmatrix}, \quad \text{for } 10 \log \left(\langle |S_{VV}|^2 \rangle / \langle |S_{HH}|^2 \rangle \right) > 2\ dB \tag{8}$$

The helix scattering expansion matrix, which takes into account of the non-reflection symmetry condition, is

$$\langle [T] \rangle_{helix} = \frac{1}{2} \begin{bmatrix} 0 & 0 & 0 \\ 0 & 1 & \pm j \\ 0 & \mp j & 1 \end{bmatrix} \tag{9}$$

The corresponding scattering powers (the surface scattering power P_s, the double bounce scattering power P_d, the volume scattering power P_v, and the helix scattering power P_c) are directly obtained from the expansion coefficients of these matrices when applied to the decomposition [8]. The decomposition takes account of an imbalance of the co-polarized channel power, $\langle |S_{HH}|^2 \rangle$ and $\langle |S_{VV}|^2 \rangle$. For the case of $\left| 10 \log \left(\langle |S_{VV}|^2 \rangle / \langle |S_{HH}|^2 \rangle \right) \right| < 2\ dB$, the power expressions become

$$P_c = f_c = 2 \left| \text{Im} \left\langle S_{HV}^* \left(S_{HH} - S_{VV} \right) \right\rangle \right| \tag{10.1}$$

$$P_v = f_v = 4\, T_{33} - 2\, P_c = 8 \langle |S_{HV}|^2 \rangle - 2\, P_c \tag{10.2}$$

$$P_s = f_s \left(1 + |\beta|^2 \right) \tag{10.3}$$

$$P_d = f_d \left(1 + |\alpha|^2 \right) \tag{10.4}$$

It should be noted here that the P_v contribution is mainly determined by the T_{33} component as seen in (10.2), which is essentially identical with the cross-polarized HV component.

The four-component scattering power decomposition algorithm, introduced in [7] and included in [3], displays the following advantages:

1. Straightforward implementation;
2. Computation time is relatively small because simple calculations are required only;
3. The decomposed powers correspond to physical scattering mechanisms, i.e., surface scattering P_s, double bounce scattering P_d, volume scattering P_v, helix (circular polarization) scattering P_c;
4. Output color-coded images are directly recognizable and easy to understand.

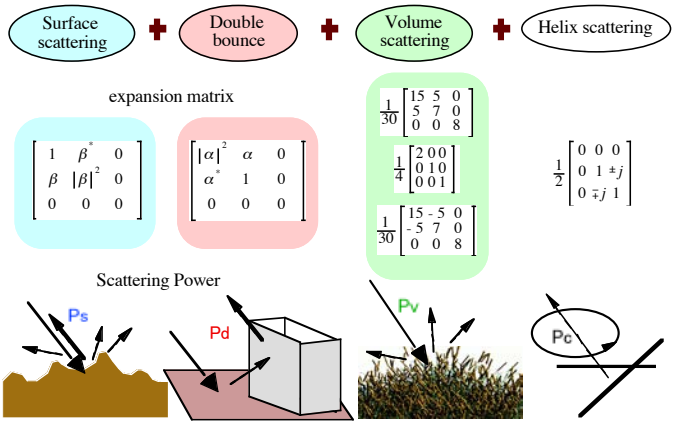

Fig. 2 The four-component decomposition of scattering powers P_s, P_d, P_v, and P_c

III. Rotation of Coherency Matrix According to the Deysing or Deorientation Concept of Huynen

In actual radar observations, the orientation direction of objects under imaging are not necessarily orthogonal to radar illumination, and the orientation direction in the transverse plane does not necessarily coincide with the radar coordinate system (H and V). For classification or decomposition purpose, it is desirable to employ a unified methodology for all objects under imaging. We employ the concept of minimization of the cross-polarized HV component also known as Deysing [9] or Deorientation [10]. This can be achieved by multiplication of the unitary rotation matrix by the rotation matrix $[R_P(\theta)]$ without loss of generality. Since the rotation of coherency matrix can be carried out with ease using mathematical formulations, we take respective advantage for the measured coherency matrix.

Assuming the measured coherency matrix to be

$$[T] = \begin{bmatrix} T_{11} & T_{12} & T_{13} \\ T_{21} & T_{22} & T_{23} \\ T_{31} & T_{32} & T_{33} \end{bmatrix} \tag{11}$$

then the coherency matrix after rotation by angle can be obtained by

$$[\, T(\theta) \,] = [R_P(\theta)] [\, T \,] [R_P(\theta)]^{\dagger} \tag{12}$$

$$[\, R_p(\theta) \,] = \begin{bmatrix} 1 & 0 & 0 \\ 0 & \cos 2\theta & \sin 2\theta \\ 0 & -\sin 2\theta & \cos 2\theta \end{bmatrix} : \text{rotation matrix} \tag{13}$$

where we denote the elements of the rotated coherency matrix as

$$[T(\theta)] = \begin{bmatrix} T_{11}(\theta)\ T_{12}(\theta)\ T_{13}(\theta) \\ T_{21}(\theta)\ T_{22}(\theta)\ T_{23}(\theta) \\ T_{31}(\theta)\ T_{32}(\theta)\ T_{33}(\theta) \end{bmatrix} \quad (14)$$

T_{33} rotation

Now, we are going to minimize the cross-polarized term in (14). As anticipated from eq. (10.2), this is the same as the minimization of the T_{33} term in (14). T_{33} can be written according to (12) as

$$T_{33}(\theta) = T_{33} \cos^2 2\theta - \mathrm{Re}\,(T_{23}) \sin 4\theta + T_{22} \sin^2 2\theta \quad (15)$$

The derivative with respect to θ is

$$T'_{33}(\theta) = 2\,(T_{22} - T_{33}) \sin 4\theta - 4\,\mathrm{Re}\,(T_{23}) \cos 4\theta \quad (16)$$

Therefore, the rotation angle can be derived from

$$T'_{33}(\theta) = 0 \quad (17)$$

This leads to the following expression for the rotation angle.

$$\tan 4\theta = \frac{2\,\mathrm{Re}\,(T_{23})}{T_{22} - T_{33}} = \frac{4\,\mathrm{Re}\left\langle S^*_{HV}\,(S_{HH} - S_{VV})\right\rangle}{\left\langle |\,S_{HH} - S_{VV}\,|^2\right\rangle - 4\left\langle |\,S_{HV}\,|^2\right\rangle} \quad (18)$$

$$2\theta = \frac{1}{2} \tan^{-1}\left(\frac{2\,\mathrm{Re}\,(T_{23})}{T_{22} - T_{33}}\right) \quad (19)$$

The expression (19) is of the same form as the phase of the correlation coefficient in the circular polarization basis [3] and [11], which is also used for surface slope estimation [11].

After this rotation, the elements of the coherency matrix become

$$T_{11}(\theta) = T_{11} \quad (20)$$

$$T_{23}(\theta) = j\,\mathrm{Im}\,(T_{23})\ ,\ T_{32}(\theta) = -\,j\,\mathrm{Im}\,(T_{23}) \quad (21)$$

$$T_{12}(\theta) = T_{12} \cos 2\theta + T_{13} \sin 2\theta\ ,\ T_{21}(\theta) = T^*_{12}(\theta) \quad (22)$$

$$T_{13}(\theta) = -\,T_{12} \sin 2\theta + T_{13} \cos 2\theta\ ,\ T_{31}(\theta) = T^*_{13}(\theta) \quad (23)$$

$$T_{22}(\theta) = T_{33} \cos^2 2\theta + T_{22} \sin^2 2\theta + \mathrm{Re}(T_{23}) \sin 4\theta \quad (24)$$

$$T_{33}(\theta) = T_{33} \cos^2 2\theta + T_{22} \sin^2 2\theta - \mathrm{Re}(T_{23}) \sin 4\theta \quad (25)$$

These eqn. (20)-(25) show how the components are re-distributed precisely. It is understood in the diagonal terms that $T_{33}(\theta)$ decreases by $\mathrm{Re}(T_{23}) \sin 4\theta$ and that $T_{22}(\theta)$ increases by the same amount, while $T_{11}(\theta)$ remains the same. It should be also noted that $T_{23}(\theta)$ becomes purely imaginary which exactly fits the helix scattering model (9) for the non-reflection symmetry condition [7] as a roll-invariant parameter [3].

IV. IV. New Four-Component Decomposition using Rotation of Coherency Matrix

A new four-component decomposition algorithm is presented in this section. The decomposition algorithm is shown in the flow-chart of Fig. 3. First, a rotated coherency matrix $[T(\theta)]$ is created by (20)-(25) using the rotation angle (19). The next step is to apply the four-component decomposition to the rotated coherency matrix $[T(\theta)]$ and to calculate the scattering powers. The helix scattering power P_c is derived at the first stage, subsequently the volume scattering power P_v is determined depending upon the magnitude balance of the co-polarized component HH versus VV as shown in the flow-chart of Fig. 3. The branch condition of the magnitude balance can be expressed as,

$$10 \log\left[\frac{\left\langle |\,b\,|^2\right\rangle}{\left\langle |\,a\,|^2\right\rangle}\right] \Rightarrow 10 \log\left[\frac{T_{11}(\theta) + T_{22}(\theta) - 2\,\mathrm{Re}\,(T_{12}(\theta))}{T_{11}(\theta) + T_{22}(\theta) + 2\,\mathrm{Re}\,(T_{12}(\theta))}\right], \quad (26)$$

in terms of the coherency matrix elements.

Once P_c and P_v are determined, P_s and P_d can be obtained by the remaining power (total power TP - P_c - P_v). The branch condition C_0 is used for determining which scattering power (P_s or P_d) is dominant based on the sign of $\mathrm{Re}\left\langle S_{HH} S^*_{VV}\right\rangle$. The expression for the branch condition C_0 can be written in terms of coherency matrix elements as

$$C_0 = T_{11}(\theta) - T_{22}(\theta) - T_{33}(\theta) + P_c \quad (27)$$

If the sign is found, it is straightforward to obtain P_s and P_d. If negative power occurs, the physical condition that all powers must be positive applies to both powers at the final stage of the algorithm in Fig. 3. Note that all terms are derivable directly from the coherency matrix elements.

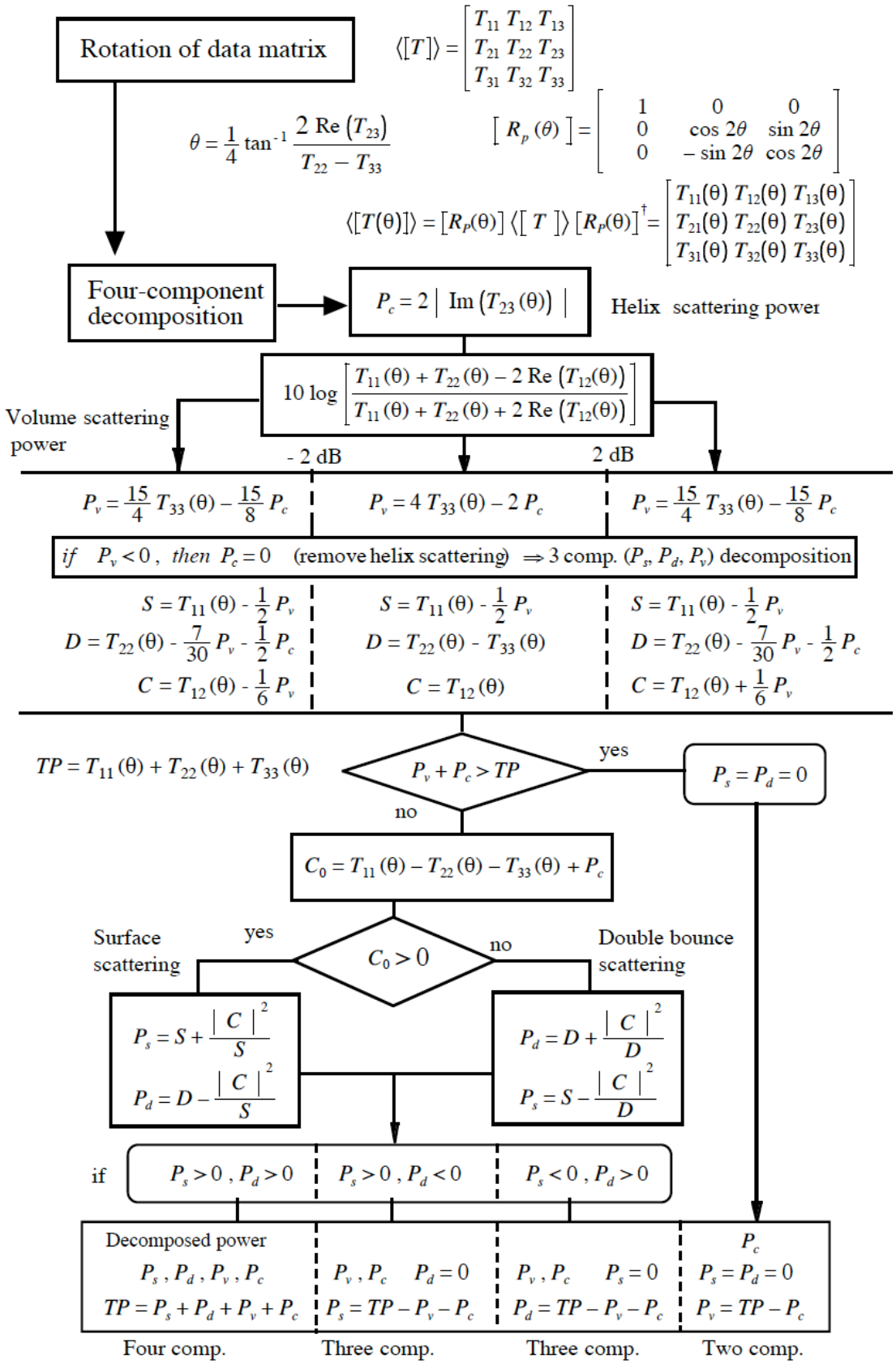

Fig. 3 Four-component scattering power decomposition algorithm using rotated coherency matrix

V. Decomposed Results and Angle Distribution

Fig. 4 shows decomposed imagery of Kyoto, Japan, before and after rotation for the sake of comparison. Fig. 1 is close-up image of Fig. 4. The Quad-pol data set used here is acquired by ALOS-PALSAR on April 9, 2009 (ALPSRP172780690_P1.1). The resolution is 30 m in the range and 5 m in the azimuth directions, respectively. The area of Kyoto contains heterogeneous objects such as oriented urban buildings in certain directions, vegetation, crop fields (dark area), mountains covered with trees, etc. Green urban area in (a) is decomposed into red or close to red or pink in the image (b). This means the oriented urban blocks turned into red (double bounce scattering) although they are oriented in different directions. The mountainous forest area became a little bit darker green after the rotation due to (25). This shows it is possible to discriminate vegetation areas from oriented urban areas by this new four-component decomposition with T_{33} rotation.

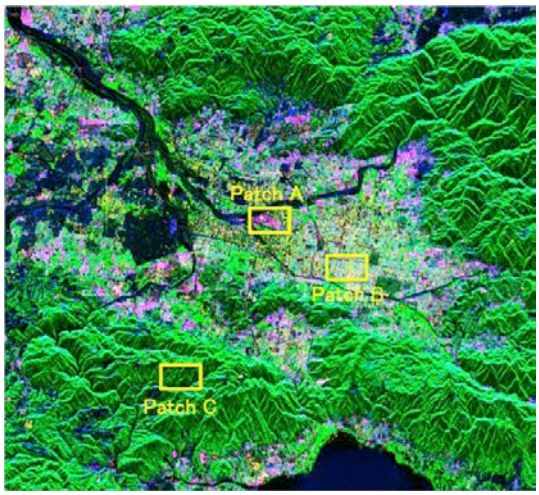

(a) Original decomposition

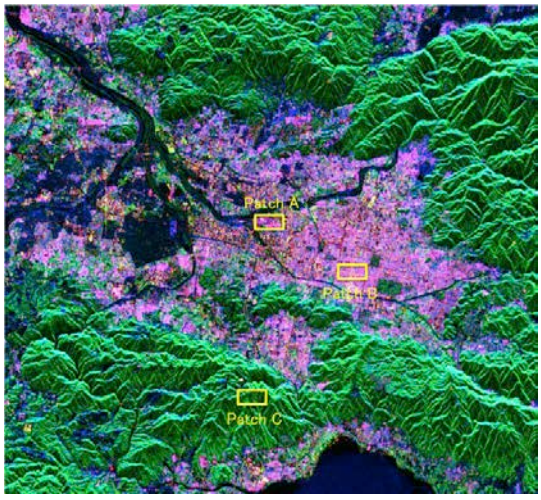

(b) Decomposition after T_{33} rotation

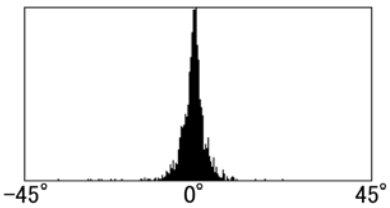

(c) Patch A: orthogonal urban

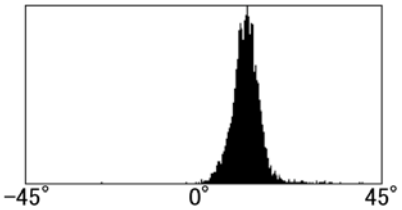

(d) Patch B: oriented urban

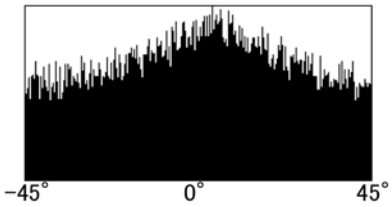

(e) Patch C: forest

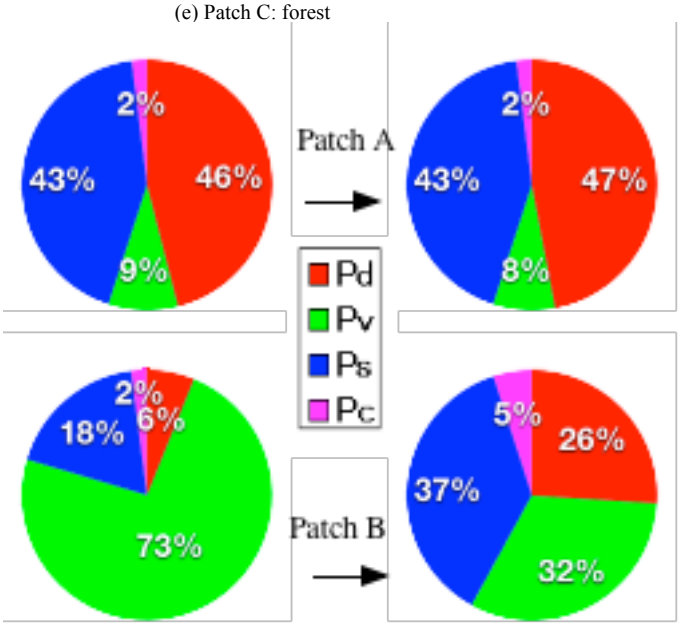

(f) Power contribution before and after rotation

Fig. 4 ALOS PALSAR Kyoto image decomposition

In order to examine these results quantitatively, the rotation angle distributions of selected patches in Fig. 4 (a) are shown in (c)-(e). The patch A and B are the same as those in Fig. 1. The angle distribution of patch A in (c) is concentrated around 0 degree for orthogonal "*red*" urban area in (a). The angle distribution of patch B of "*oriented urban*", yields the peak at 10 degrees in (d) which is consistent with the actual situation (12 degrees by Google Earth image), whereas the angle is distributed rather randomly (e) for patch C in the forested area.

Figure 4 (f) shows the decomposed power contributions

before and after T_{33} rotation. It is seen in Patch A that the ratio of each power does not change, however, that in Patch B that the volume scattering power P_v reduces and the surface/double bounce scattering powers (P_s and P_d) increase. Since the patch B contains oriented urban blocks, the rotation effect considerably increases the decomposition performance.

The window size for the ensemble average in image processing was chosen as 2 in the range direction and 12 in the azimuth direction which corresponds to 60 m by 60 m in the ground area. This size 2 x 12 was found to be the best for ALOS Quad-pol data sets for the decomposition among 1 x 4, 1 x 6, 2 x 6, 2 x 12. It should be noted that this rotation of coherency matrix is carried out in a selected window, we obtain the rotation angle as a result of second order statistics. If there is a strong point scatterer compared to the surroundings in the imaging window, the scattering powers are merged and averaged in the window.

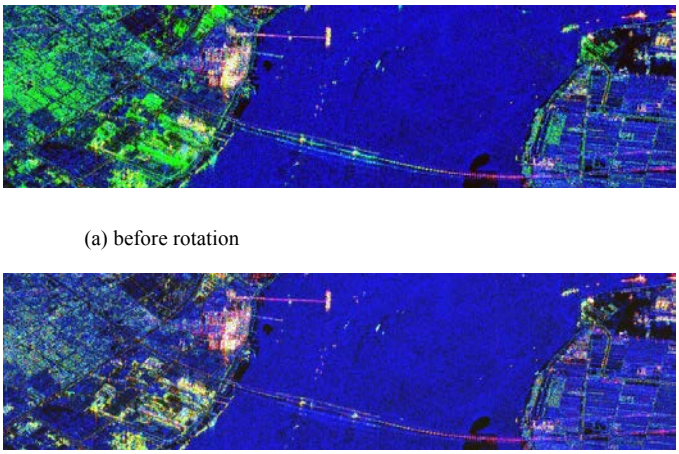

(a) before rotation

(b) after rotation

Fig. 5 Sutong Changjiang Highway Bridge near North Shanghai, China (a) before rotation, (b) after rotation

VI. Decomposed Images of Other Scenes

This new four-component decomposition scheme is also applied to many other ALOS-PALSAR quad-pol. images to verifying the correct implementation of this novel scheme. For example the scene shown in Fig. 5 is North-Shanghai (data no. ALPSRP170890630). This image contains various interesting objects, i.e., the bridge itself (Sutong Changjiang Highway Bridge, 8206 m long, built on June 30, 2008) and arbitrarily oriented building blocks near the bridge. The green color produced by the bridge in (a) turned into both red and blue color with details more easily distinguishable in (b). The bottom reflection line among three lines of the bridge on the river surface might be a fake double bounce scattering (yet green color) on the river surface [13]. It faded away in the rotated decomposition, creating a bridge image more straightforwardly to interpret. The big oriented building blocks near the bridge (left corner) are decomposed into man-made structures with mixture of several components. It is possible to see finer structures showing double bounce (*red lines*) in the rotated image (b). Other man-made structures are again decomposed correctly although they are decomposed as volume scattering objects in the original decomposition. It is seen that the rotated data yields the most appropriate decomposition result.

In order to provide further verification of the introduced rotation scheme, another complementary image is provided in Fig. 6. The area is the western part of Niigata-city, Japan, located at 37.53.16N, 138.59.50E. The color-coded images are obtained from the data sets acquired with the airborne L-band Pi-SAR with resolution of 3 by 3 meters on the ground. The window size was chosen to be 5 by 5 pixels in this L-band data. The window size is determined after the examination of convergence of the second order statistics together with taking into account the resolution.

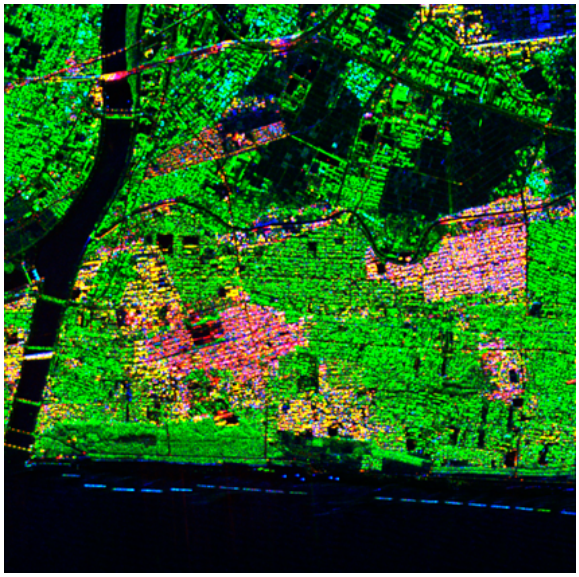

(a) before rotation

(b) after rotation

Fig. 6 L-band Pi-SAR image of West Niigata, Japan

It is seen in Fig. 6 that "*green*" in almost all areas in (a) turned into "*red*," except for local pine tree sections close to the Japan Sea at the bottom. Note that "*red*" area in (b) while "*green*" in (a), are residential houses with some mixture of vegetation. On the other hand, bright "*red*" areas in (a) are enhanced in (b) because they are directed almost orthogonal to radar illumination. It is interesting to see bridges over the river (left in the image) are also turned into "*red*" indicating double bounce structures consisting of water surface and bridge side walls. Since the scene imaged in this Fig. 6 is close to Niigata University, we were able to check the validity of the new decomposition result most carefully.

VII. Conclusion

This paper presented an improvement to a decomposition scheme implementing a rotation of the coherency matrix before carrying out the four-component decomposition. By minimizing the cross-polarized component, the rotation angle is retrieved. Using the recovered angle the coherency matrix is rotated. The decomposition algorithm provided in this paper uses the coherency matrix elements only. This method is quite simple and effective. It is successfully carried out subject to fully polarimetric SAR data sets and enables discrimination of oriented urban blocks versus vegetation as different scattering objects which previously were difficult to be discriminated. Arbitrarily oriented urban areas are then correctly classified into double bounce man-made structures. In addition, the image quality increased compared with the original decomposition within the fixed specification frame of radar resolution.

Since this rotation of coherency matrix is carried out based on the ensemble average of polarimetric scattering characteristics in a selected imaging window, we obtain the rotation angle as a result of second order statistics. If there is a strong point scatterer compared to the surroundings in the imaging window, the polarimetric characteristics of the strong scatterer are merged and averaged in the window.

Acknowledgment

The authors are grateful to JAXA for providing outstanding and well calibrated ALOS-PALSAR and Pi-SAR Quad-pol data sets.

References

[1] [Online]. Available: http://www.eorc.jaxa.jp/ALOS/en/about/palsar.htm
[2] [Online]. Available: http://www.palsar.ersdac.or.jp/e/index.shtml
[3] J. S. Lee and E. Pottier, *Polarimetric radar imaging from basics to applications*, (398 pages), CRC Press, 2009
[4] S. R. Cloude and E. Pottier, "A review of target decomposition theorems in radar polarimetry," *IEEE Trans. Geosci. Remote Sens.*, vol. 34, no. 2, pp. 498-518, Mar. 1996.
[5] E. Pottier, and J. S. Lee, "Application of the <<H/A/$\overline{\alpha}$>> polarimetric decomposition theorem for unsupervised classification of fully polarimetric SAR data on the Whishart distribution," *Proceedings of EUSAR2000*, pp. 265-268, May 2000
[6] A. Freeman, and S. Durden, "A three-component scattering model for polarimetric SAR data," *IEEE Trans. Geosci. Remote Sens.*, vol. 36, no. 3, pp. 963-973, May 1998.
[7] Y. Yamaguchi, T. Moriyama, M. Ishido, and H. Yamada, "Four-component scattering model for polarimetric SAR image decomposition," *IEEE Trans. Geosci. Remote Sens.*, vol. 43, no. 8, pp. 1699-1706, Aug. 2005.
[8] Y. Yajima, Y. Yamaguchi, R. Sato, H. Yamada, W. -M. Boerner, "POLSAR image analysis of wetlands using a modified four-component scattering power decomposition," *IEEE Trans. Geosci. Remote Sens*., vol. 46, no. 6, pp. 1667-1773, 2008
[9] J. R. Huynen, Phenomenological theory of radar targets, Ph.D Thesis, University of Technology, Delft, The Netherlands, 1970
[10] F. Xu, and Y. Q. Jin, "Deorientation theory of polarimetric scattering targets and application to terrain surface classification," *IEEE Trans. Geosci. Remote Sens.*, vol. 43, no. 10, pp. 2351-2364, Oct. 2005.
[11] J. S. Lee, D. L. Schuler, T. L. Ainsworth, E. Krogager, D. Kasilingam, W. -M. Boerner, "On the estimation of polarization orientation shifts induced by terrain slopes," *IEEE Trans. Geosci. Remote Sens.*, vol. 40, no. 1, pp. 30-41, Jan. 2002.
[12] Y. Yamaguchi, *Radar polarimetry from basics to applications* (in Japanese, 182 pages), IEICE, 2007
[13] J. S. Lee, E. Krogager, T. L. Ainsworth, W. -M. Boerner, "Polarimetric analysis of radar signature of a manmade structure," *IEEE Geosci. Remote Sens. Letters*, vol.3, no. 4, pp. 555-559, Oct. 2006.

Yoshio Yamaguchi (M'83-SM'94-F'02) received the B.E. degree in electronics engineering from Niigata University in 1976, and the M.E. and Dr. Eng. Degrees from Tokyo Institute of Technology in 1978 and 1983, respectively. In 1978, he joined the Faculty of Engineering, Niigata University. From 1988 to 1989, he was a Research Associate at the University of Illinois at Chicago. His interests are in the field of radar polarimetry, microwave sensing and imaging. He has served as Chair of IEEE GRSS Japan Chapter (02-03), Chair of URSI-F Japan (06-11), and Associate editor for Asian affairs of GRSS Newsletter (03-07). He is a Fellow of IEICE, Japan, and a recipient of 2008 IEEE GRSS Education Award.

Akinobu Sato received the B.E. and M.E. degrees in Information Engineering from Niigata University, Japan, in 2009 and 2011, respectively. He was a graduate student of Niigata University where he had been engaged in POLSAR image analysis.

Ryoichi Sato (M'04) received the B.S., M.S. and Ph.D. degrees in electrical engineering from Chuo University, Tokyo, Japan, in 1992, 1994 and 1997, respectively. Since April 1997, he has been with the Faculty of Education and Human Sciences, Niigata University, Japan, where he is currently an associate professor. In 2002, he was a Research Scholar at Polytechnic University, Brooklyn, NY. His current research interests are electromagnetic wave propagation, FDTD analysis, polarimetric image analysis.

Wolfgang-Martin Boerner (SM'75-F'84-LF92) received the Ph.D. degree from The University of Pennsylvania, in 1967. From 1967 to 1968 he was with the University of Michigan. In 1968 he joined the University of Manitoba. Since 1978, he has been a Professor at the Department of Electrical & Computer Engineering, the University of Illinois at Chicago. His research interests are Electromagnetic Vector Inverse Scattering, Radar Polarimetry, Polarimetric Interferometry and Tomography. He is a member of numerous international scientific societies: Senior member of CAP, ASEE, ASRSP &ISRSP, Fellow of IEEE, OSA, SPIE, AAAS, IEICE. He is a member of the honor societies Sigma Xi, the American and the German Fulbright Associations, and the Alexander von Humboldt Association.

Hiroyoshi Yamada (M'93) received the B.E., M.E., and Dr. Eng. degree from Hokkaido University, Japan, in 1988, 1990, and 1993, respectively, all in electronic engineering. In 1993, he joined the Faculty of Engineering, Niigata University, where he is an associate Professor. From 2000 to 2001, he was a visiting scientist at Jet Propulsion Laboratory, California Institute of Technology, Pasadena, CA. His interests involve in the field of array signal processing, polarimetric radar interferometry, high resolution techniques. He is a member of IEICE of Japan and a recipient of 2010 best paper award of IEICE.